

European Geosciences Union General Assembly 2012

Vienna, Austria, 22-29 April 2012

Session AS2.2/OS5.3: Turbulence in the atmospheric  
and oceanic boundary layers, Vol. 14, EGU2012-12716

## Zone of flow establishment in turbulent jets

Dimitriadis P., M. Liveri-Dalaveri, A. Kaldis, C. Kotsalos, G.  
Papacharalampous and P. Papanicolaou

Department of Water Resources and Environmental Engineering  
National Technical University of Athens

([www.itia.ntua.gr](http://www.itia.ntua.gr))

# 1. Abstract

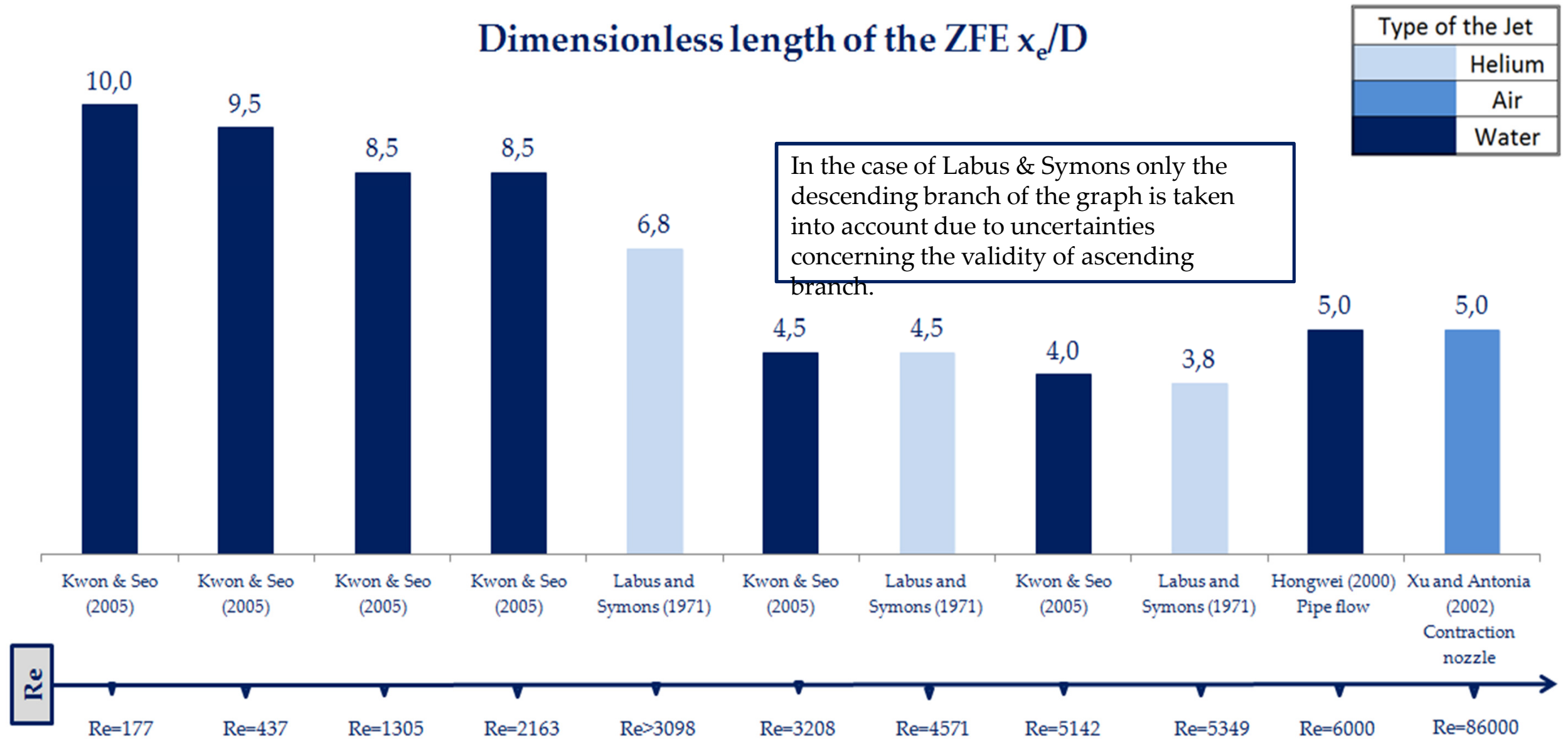
It is well established experimentally that as the Reynolds number increases the core of the jet diminishes and has smaller effects on the jet's mean profiles (e.g. concentration, temperature, velocity). The scope of this project is to examine this relationship based on dimensional analysis and experimental data. For that, spatio-temporal concentration records are obtained on the plane of symmetry of heated vertical round jets (for a laboratory turbulent scale at the order of mm) using tracer concentration measurements via a planar laser induced fluorescence technique (PLIF). The investigation area is set close to the nozzle of the jets (up to 10 jet diameters away), at the zone of flow establishment (ZFE), so as to determine the geometric characteristics (dimensions and shape) of the core as a function of the initial velocity and nozzle diameter. The ZFE is estimated through the absence of turbulent intensity fluctuations (assuming a threshold value of 1% of the maximum intensity).

# 2. Introduction

The jets are widely used in several engineering fields mainly for wastewater/salt disposal, gaseous releases etc. Using engineering terms, investigation of the zone of flow establishment (ZFE) “seems both futile and unnecessary in view of its limited extent” (Jirka, 2004).

Nevertheless, in scientific terms, it is of high importance as it includes the shear layer and transition to turbulence. The ZFE is defined as the area within the shear layer developed at the edge of a jet and is known to have a ‘conical’ shape, because of the shear layer dispersion towards the jet axis at the advancing of the jet (Chen & Nikitopoulos, 1979). The limit of that dispersion is the axis of symmetry and its distance from the nozzle is considered as the ZFE length ( $x_e$ ), which is affected by flow instability and thus it is difficult to define. It is generally observed that as the Reynolds number increases, distance  $x_e$  decreases. A literature survey is done along with some measurements of  $x_e$  in time and space via PLIF visualization to verify this view. Specifically, three locations are recorded that are based on the time-averaged (TAV) and root-mean-squared (RMS) images of rhodamine 6G concentration  $C$ . The first at the point where the TAV of  $C$  at the jet-axis starts to decay ( $x_{e,m}$ ), the second where the RMS of  $C$  takes values above a threshold ( $x_{e,smin}$ ), and the third where the normalized RMS of  $C$  ( $x_{e,smax}$ ) is maximum.

# 3a. Literature survey (experimental values)



Researchers	$x_e/D$	Re	Type of the Jet
Albertson et al. (1948)	6,2	large	Air
Crow and Champagne (1971)	5,3	large	Water
Pratte and Baines (1967)	6,4	large	Air

Figure 1a (up): Experimental values of the ZFE length are extracted from the graphs of the researchers noted above with a certain degree of tolerance. The axes of the graphs are  $V/V_0$  and  $x_e/D$ , where  $V$  is the mean axial jet-velocity and  $D$  the nozzle's diameter (where the subscript 0 denotes the exit of the orifice).

Figure 1b (left): Several researchers have measured the ZFE length indicating only the order of the Reynolds number (Re).

## 3b. Literature survey (approximated equations)

- Abramovich (1963) states that for a jet of an incompressible fluid in a co-flowing ( $V \uparrow \uparrow u_a$ , the cross flow ambient velocity) external stream, the ZFE length is given by the equation :

$$x_e / D = \pm \frac{1}{2} \frac{1 + V / u_a}{0.27(1 - V / u_a)(0.416 + 0.134V / u_a)}, \text{ where minus sign for } V / u_a > 1$$

- Pratte & Baines (1967) report that  $x_e$  of a jet released from a tube perpendicular to a cross flow approaches the potential core length for a turbulent free jet with no cross flow, as the ratio of the jet velocity to the cross-flow velocity ( $V/u_a$ ) becomes large. Although  $x_e$  is also a function of the Reynolds number (in the tube), Reynolds number dependence is less important for large release momentum. Pratte and Baines (largest Reynolds number-vertically directed jet) data are correlated as:

$$x_e / D = 6.4(1 - \exp(-0.48(V / u_a))), \text{ for } u_a = 0 : x_e / D = 6.4$$

- Chen & Nikitopoulos (1979) present some data for  $x_e$ , derived from a differential model, as a function of the densimetric Froude number ( $F_o$ ), for a plume discharging vertically into a stagnant ambient. Henderson-Sellers (1983) suggest the following empirical fit to these data:

$$x_e = \begin{cases} 4D, & F_{oT}^2 < 8 \\ \left(3.27 + 0.26\sqrt{F_{oT}^2}\right)D, & 8 \leq F_{oT}^2 \leq 128, \\ 6.2D, & F_{oT}^2 > 128 \end{cases}, \text{ where } F_{oT}^2 = \frac{V^2}{\frac{D}{2} \frac{g}{T_a} \Delta T}, \text{ where } \begin{cases} \Delta T = T_0 - T_\alpha, \\ T(^{\circ}\text{C}) \text{ is the temperature,} \\ \text{a subscript is for the ambient} \\ \text{and 0 the exit of the nozzle} \end{cases}$$

### 3c. Literature survey (approximated equations)

- Lee & Jirka (1981) have given a solution of  $X_e$  as a function of  $F_0$  for a stagnant uniform waterbody of large horizontal extent.  $X_e$  increases rapidly from zero for  $F_0 \rightarrow 0$ , to an asymptotic value of 5.74 for  $F_0$  greater than 25. This is somewhat smaller than the value of 6.2 determined by Anderson et al. (1950).

$$1 + \frac{4}{F_0^2} \left( \frac{X_e}{12} + \frac{\sqrt{\pi} \lambda \epsilon}{12} X_e^2 + \frac{\lambda^2 \epsilon^2}{3} X_e^3 \right) = \frac{(1 + \lambda^2)^2}{8 \lambda^4 \epsilon^2} \frac{1}{X_e^2}, \text{ where}$$

$X_e = x_e / D$ , the ZFE length normalized around the diameter

$\epsilon = 0.109$ , jet spreading angle

$\lambda = 1.14$ , ratio of temperature diffusion thickness to momentum diffusion thickness

- According to Jirka (2004) the ZFE length is measured from a linear spread of the shear layer and estimated about  $6.2 D$ , based on velocity profiles, or about  $5D$ , based on scalar profiles, due to the typical dispersion ratio,  $\lambda > 1$ . This fundamental result is generalized for cross-flow effects using the empirical approach of Schatzmann (1978), and for buoyancy effects through model formulation by Lee & Jirka (1981). They suggest

$$x_e = 5D \left( 1 - 3.22 \frac{\sin \gamma_0}{V / u_a} \right) \left( 1 - e^{-2.0(F_0/4.67)} \right), \text{ where } \gamma_0 = \sin^{-1} \left( \sqrt{1 - \cos^2 \theta_0 \sin^2 \sigma_0} \right) \text{ with}$$

$\sigma_0$ , the angle measured counterclockwise from the ambient current direction

to the plane projection of the orifice centerline and

$\theta_0$ , the angle between the orifice centerline and the horizontal plane.

Note that for  $u_a = 0$ :  $x_e = 5D \left( 1 - e^{-2.0F_0/4.67} \right)$

## 4. Experimental set-up

An experiment using planar laser-induced fluorescence (PLIF) visualization is set at the laboratory of Applied Hydraulics of the NTUA in order to determine the geometric characteristics (intrusion length and shape) of the core. The experiment is set-up as follows:

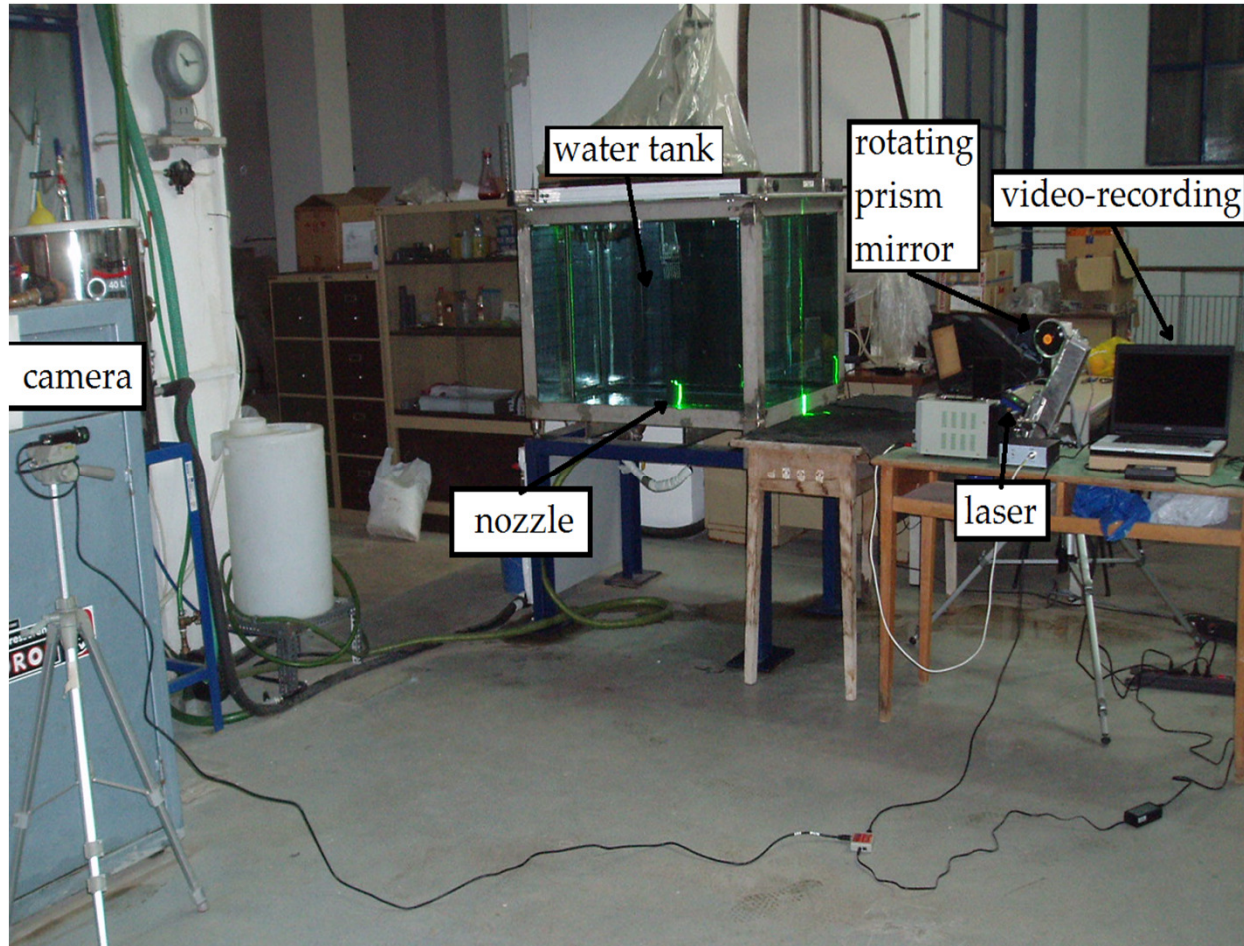


Figure 2: PLIF experimental set-up (NTUA, Laboratory of Hydraulics)

The camera is set at the plane of symmetry of the jet, at a distance of at least  $0.75 \times D$  meters from the nozzle, so as to achieve a window-view height greater than 10 diameters. The width of the window is chosen to be at least 3 diameters long to capture the jet expansion (at an angle of  $12^\circ$ - $15^\circ$  with respect to jet axis). Each video lasts around 25 sec, and is recorded at 12 frames per second (fps), so as to achieve stationarity.

- A jet is heated (buoyant) and dyed with a rhodamine 6G (R6G) substance and then exits from a nozzle of diameter  $D$  to ambient water of lower temperature.
- A DPSS 1 W laser beam, at 532 nm wavelength (green), is converted to a thin laser light sheet via a rotating prism mirror (at 20 kHz). R6G emits 556 nm light (yellow) when excited by the 532 nm light making visualization possible.
- A high resolution video-camera is then used to videotape the flow field. In this manner, the light intensity of R6G (measured through the RGB 8bit frame format of the camera) can be converted to concentration.

# 5. Calibration

The initial fluorescence light intensity  $I_0$  can be assumed to be proportional to the R6G initial concentration  $C_0$  for values less than 50  $\mu\text{g/l}$  (Ferrier et al., 1993). A decrease in power and light intensity occurs as the laser beam enters the water tank and travels through the dyed jet. For this range of concentrations and over a small path length (of order of 1 cm), the power attenuation can be assumed to be negligible (Walker, 1987). Thus, only the light intensity attenuation factor is taken into account and the raw data are modified according to Walker (1987) formula :

$$I(x) = I_0 e^{-\sum \eta_I x_i}, \text{ with } \eta_I = \eta_{Iw} + \varepsilon_I C, \text{ where}$$

$x_i$  is the distance the laser beam travels through water (from pixel  $i-1$  to  $i$ ),

$\eta_{Iw}$  and  $\varepsilon_I$  are the laser beam attenuation coefficients through water and R6G, respectively.

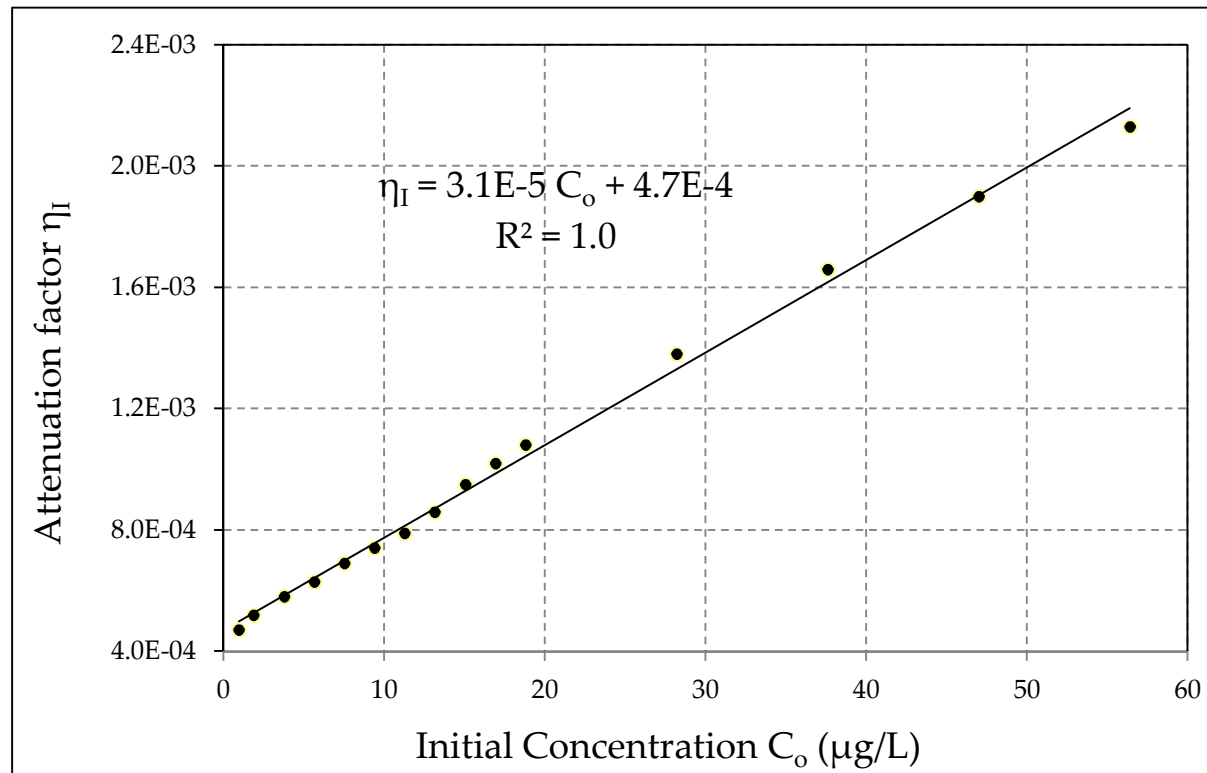


Figure 3: Light intensity attenuation factor, where  $\varepsilon_I$  is the slope ( $3.1 \cdot 10^{-5}$ ) and  $\eta_{Iw}$  the intercept ( $4.7 \cdot 10^{-4}$ ) of the trendline.

- Measurements within an adequate range (1-60  $\mu\text{g/l}$ ) of concentration intensities (fully mixed into the water tank) are made in order to determine the attenuation coefficients  $\varepsilon_I$  and  $\eta_{Iw}$  (as shown in figure 3).
- The red intensity of the RGB color format and a shutter speed (SS) of 50 msec are chosen as the optima, based on image resolution and data quality criteria.
- The image scale  $Sc$  and lens' distortion (pixel size variation along height) are estimated from a ruler placed on the nozzle. The average value of  $Sc$  is considered as it only varies  $\approx 2\%$ .

## 6. Data processing

- Four jet diameters are tested (0.5, 1, 1.5 and 2 cm) for a range of initial discharges ( $Q$ ) 5 to 40  $\text{cm}^3/\text{s}$  ( $\pm 0.85 \text{ cm}^3/\text{s}$ ) with Reynolds numbers  $\text{Re} = 10^2 \div 10^4$  and Froude numbers  $F_0 = 1 \div 200$ .
- Flow instabilities occurring within the ZFE may result in a non axisymmetric jet:
  - a) Noise from the camera (estimated via recording with the camera lens covered), background noise (estimated via recording with no jet discharge) and noise from slow motion of ambient water (observed from suspended particles) is estimated to be less than 1% (fig. 6).
  - b) A fountain-like periodic movement of the core is observed within the ZFE.
- The length and shape of the core are estimated through the absence of turbulent intensity fluctuations rather than the presence of a constant initial jet concentration. This is achieved by the standard deviation image rather than the mean or the instantaneous one. Image and data processing are done using MATLAB<sup>®</sup>.

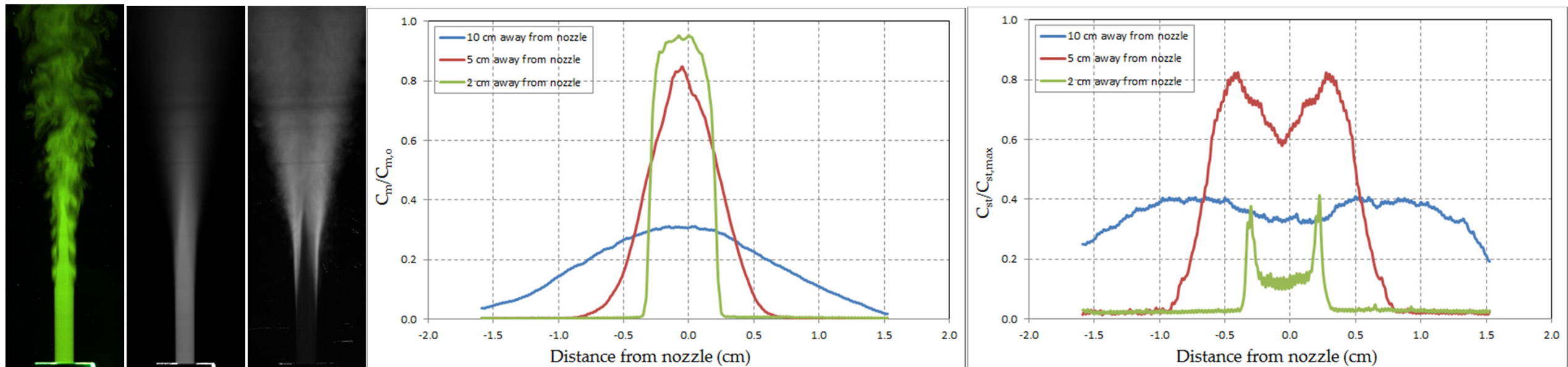


Figure 4: Instantaneous, time-averaged and RMS images (green and gray images, left). Normalized mean and standard deviation distributions with their maximum values (middle and right figure, respectively) at a distance of 2 cm (within the ZFE), 5 cm (around the end of ZFE) and 10 cm (outside the ZFE) from the nozzle.

# 7. Experiments performed

Here, the initial conditions of the conducted experiments as well as the measured  $x_e$ , are

Symbol memo		Exp1		No	1	2	3	4	5	6	7	8	9	10	11	12	13	14	15	16 <sup>2</sup>	17 <sup>2</sup>			
o	value from digital analysis of image	D (cm)	0.5	Frames	360	244	508	508	510	521	511	509	510	507	508	473	449	515	621	459	508			
		Sc (cm/pxl)	0.0125	Q (ml/s)	5.2	6.0	6.9	8.6	10.2	11.9	13.6	15.3	16.9	18.6	22.0	25.3	28.7	32.0	35.4	35.4	35.4			
		SS (msec)	50	Re	1418	1646	1875	2331	2788	3244	3700	4157	4613	5070	5983	6896	7809	8721	9634	9634	9634			
^	value from digital analysis of image (with small disturbances <sup>5*</sup> )	Frq (frs/sec)	12.0	Fr	28.5	33.1	37.7	46.8	56.0	65.2	74.4	83.5	92.7	101.9	120.2	138.6	156.9	175.3	193.6	193.6	193.6			
		T <sub>jet</sub> (°C)	23.3	x <sub>e,s</sub> min (cm)	4.6o	2.2o	1.8o	1.1o	1.1o	1.3o	1.2o	1.0^	-	-	0.8o	0.9o	0.9o	0.9^	0.9^	1.1o	1.5o			
		T <sub>amb</sub> (°C)	14.1	x <sub>e,m</sub> (cm)	6.2o	4.2o	3.1o	2.7o	2.4o	2.1o	2o	1.9o	1.6o	1.4^	1.2o	1.1^	1.1o	1.1o	1.7o	1.7o	1.7o			
		g <sub>o</sub> '	1.732	x <sub>e,s</sub> max (cm)	8.7o	5.5o	3.9o	3.7o	3.3o	3o	2.9o	2.4^	-	-	3.9o	2.8o	2.5o	2.5^	2.6^	3.1o	2.5o			
^	value from digital analysis of image (with medium disturbances <sup>5*</sup> )	Exp2		No	1	2	3	4	5	6	7	8	9	10	11	12	13	14	15	16	17	18	19	20
		D (cm)	1.0	Frames	303	308	305	306	409	307	309	305	307	308	342	308	310	304	307	338	339	316	304	306
		Sc (cm/pxl)	0.0125 <sup>1</sup>	Q (ml/s)	5.2	6.9	8.6	10.2	11.9	13.6	15.3	16.9	18.6	20.3	22.0	23.6	25.3	27.0	28.7	30.3	32.0	33.7	35.4	37.1
#	value from digital analysis of image (with C/Co<<1 at the ZFE <sup>6*</sup> )	SS (msec)	50	Re	781	1033	1284	1536	1787	2038	2290	2541	2793	3044	3296	3547	3799	4050	4302	4553	4804	5056	5307	5559
		Frq (frs/sec)	12.0	Fr	4.4	5.8	7.2	8.6	10.0	11.4	12.8	14.2	15.6	17.0	18.4	19.8	21.2	22.6	24.0	25.4	26.8	28.2	29.6	31.0
		T <sub>jet</sub> (°C)	27.5	x <sub>e,s</sub> min (cm)	6.4o	6.3o	3.8^	4.9o	3.9o	4.3o	3.8o	3o	3.3o	3.3o	2.9o	2.8o	3.1o	2.7o	2.9o	3.1o	2.7o	3o	1.9o	-
!	value from graphical analysis of image (no possibility of digital analysis)	T <sub>amb</sub> (°C)	17.1	x <sub>e,m</sub> (cm)	10o	9.7o	9.1o	6o	5.4o	5.2o	5.5o	4.6o	4.7o	4.3o	4.6o	4.2o	4.3o	4.1o	4.1o	4.2o	4.5o	4.8o	4.8o	-
		g <sub>o</sub> '	2.312	x <sub>e,s</sub> max (cm)	-	-	-	7.7!	6.2o	6.2^	6.6o	6.6!	6.2^	5.2!	5.2!	6.1!	5!	5!	5!	5!	5.2^	5.7^	-	-
		Exp3		No	1	2	3	4	5	6	7	8	9	10	11	12	13	14	15	16	17	18	19	
o	value from graphical analysis of image (no possibility of digital analysis)	D (cm)	1.5	Frames	312	308	395	343	316	307	309	572	308	318	308	309	308	308	365	307	329	309	289	
		Sc (cm/pxl)	0.0227 <sup>1</sup>	Q (ml/s)	5.2	8.6	10.2	11.9	13.6	15.3	16.9	18.6	20.3	22.0	23.6	25.3	27.0	28.7	30.3	32.0	33.7	35.4	37.1	
		SS (msec)	50	Re	520	854	1022	1189	1356	1523	1691	1858	2025	2192	2360	2527	2694	2862	3029	3196	3363	3531	3698	
o	value from graphical analysis of image (no possibility of digital analysis)	Frq (frs/sec)	12.5	Fr	1.6	2.6	3.1	3.6	4.2	4.7	5.2	5.7	6.2	6.7	7.2	7.7	8.2	8.8	9.3	9.8	10.3	10.8	11.3	
		T <sub>jet</sub> (°C)	27.4	x <sub>e,s</sub> min (cm)	6o	7.1o	7.8o	5.3o	4.4o	4.5o	5o	4.1o	3.2o	3.5o	3.2o	4.5o	3o	4o	3.7o	3.5o	3.3o	3.5o	2.6o	
		T <sub>amb</sub> (°C)	17.1	x <sub>e,m</sub> (cm)	7.6o	8.2o	8.2o	8.2o	7.3o	7.0o	7.8o	6.0o	5.8o	7.6o	8.3o	8.2o	8.3o	7.6#	8.2#	7.8#	8.8#	8.4#	9.3#	
-	no possibility of digital neither graphical analysis	g <sub>o</sub> '	2.286	x <sub>e,s</sub> max (cm)	9.8o	10.5o	10.6o	10.6o	10o	9.1!	10.3!	7.8o	7.7^	8.9!	8!	7.9^	7.5!	7.8!	7.2!	7.6o	7.6!	-	7.5!	
		Exp4		No	1 <sup>4</sup>	2	3	4	5 <sup>4</sup>	6 <sup>4</sup>	7	8	9	10 <sup>4</sup>	11 <sup>4</sup>	12								
		D (cm)	2.0	Frames	294	529	222	312	551	508	509	264	163	332	303	6								
-	no possibility of digital neither graphical analysis	Sc (cm/pxl)	0.025	Q (ml/s)	5.2	6.9	8.6	10.2	11.9	13.6	18.6	22.0	25.3	28.7	35.4									
		SS (msec)	75 <sup>3</sup>	Re	345	456	567	678	789	900	1233	1455	1677	1900	2122	2344								
		Frq (frs/sec)	12.0	Fr	1.020	1.349	1.677	2.005	2.334	2.662	3.647	4.304	4.961	5.618	6.274	6.931								
-	no possibility of digital neither graphical analysis	T <sub>jet</sub> (°C)	21.9	x <sub>e,s</sub> min (cm)	11.2o	19.1o	3.4o	-	6.7o	4.0o	2.6o	6.5o	5.1o	4.2o	3.3o	3.0o								
		T <sub>amb</sub> (°C)	15.0	x <sub>e,m</sub> (cm)	13.4^	-	4.9^	8.1^	10.2^	9.4^	5.8^	7.3^	6.6^	5.7^	5.3^	4.4^								
		g <sub>o</sub> '	1.320	x <sub>e,s</sub> max (cm)	16.5o	20.4o	7.4o	-	12.5o	10.3o	11o	10.4o	9.2o	8.4o	8.2!	7.4o								

1\* Average value of SC.  
 2\* Same discharge but different SS (25 msec for the 16<sup>th</sup> experiment and 10 for the 17<sup>th</sup> one.  
 3\* The SS differs from the previous experiments.  
 4\* The recording speed was not stable throughout the experiments because of computer memory issues.  
 5\* Disturbances are considered exogenous factors (e.g. dirt/scratch on the water-tank's glass).

## 8a. Experimental results (geometrical ZFE shape)

The outline limit of the ZFE is shown below. The geometrical shape of the ZFE is close to a conical one (for the instantaneous and time-averaged images) and to a ballistic one (for the RMS image). One can observe from the RMS image, that flow fluctuation (turbulence) is initiated at jet nozzle elevation. This is not easy to observe from the two other images, therefore one can erroneously claim that transition to turbulence occurs at higher elevations.

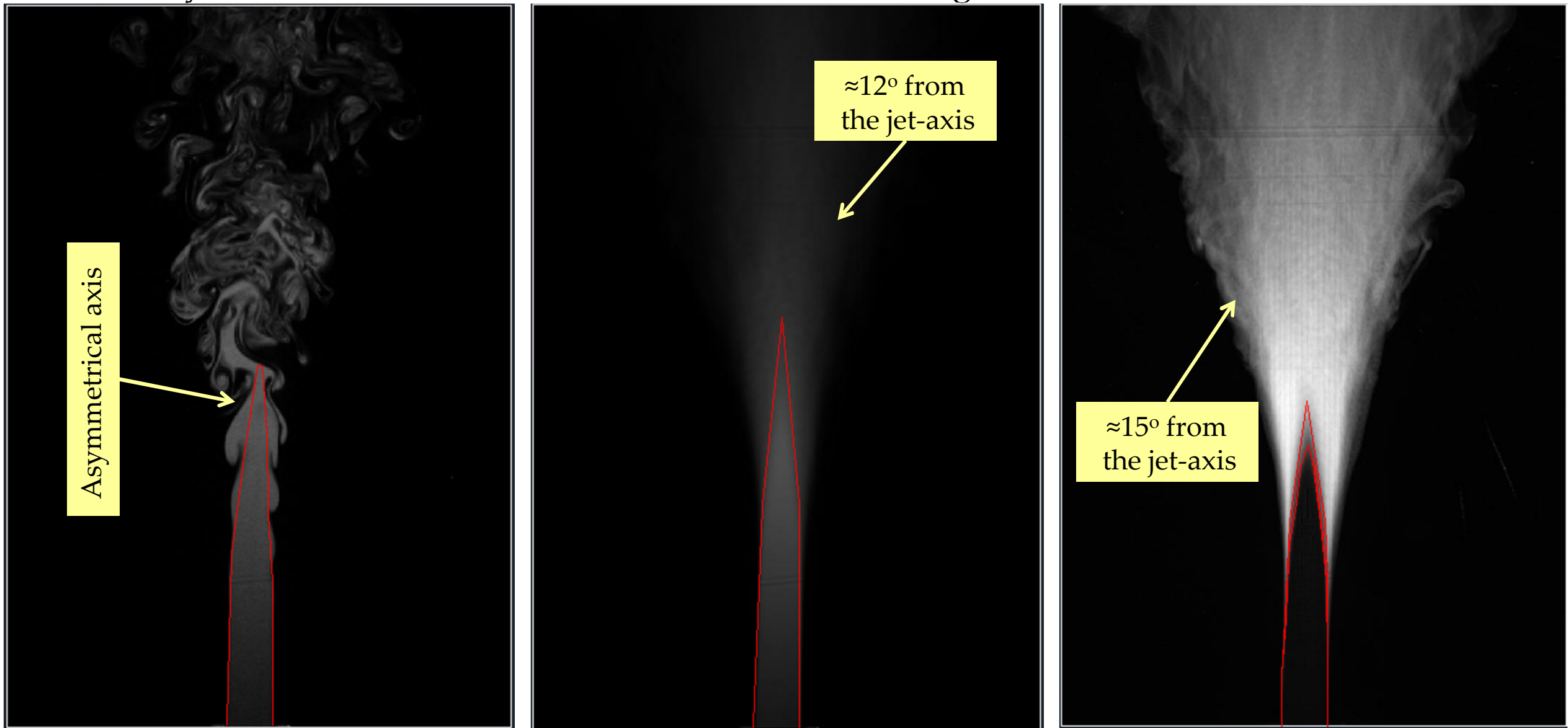


Figure 5: Outer limits (red color line) of the ZFE in an instantaneous (left), time-averaged (middle) and RMS (right) images (here, the inner line is shown as well). These images are taken from the 3<sup>rd</sup> experiment ( $D=1.5$  cm). Scale is 1:2.

## 8b. Experimental results (ZFE length)

The mean and standard deviation distributions of the concentration along the jet-axis are shown below. The mean concentration should be constant within the ZFE but here is rising probably due to the fact that the initial concentration of R6G ( $\approx 50\mu\text{g/l}$ ) is high for the laser to pass through in a small area around the nozzle. Also, the distributions of the standard deviation do not show a successive decrease. This is because they are normalized with the maximum standard deviation observed within the ZFE which varied (measured 30 to 45% of the  $C_{m,o}$ ).

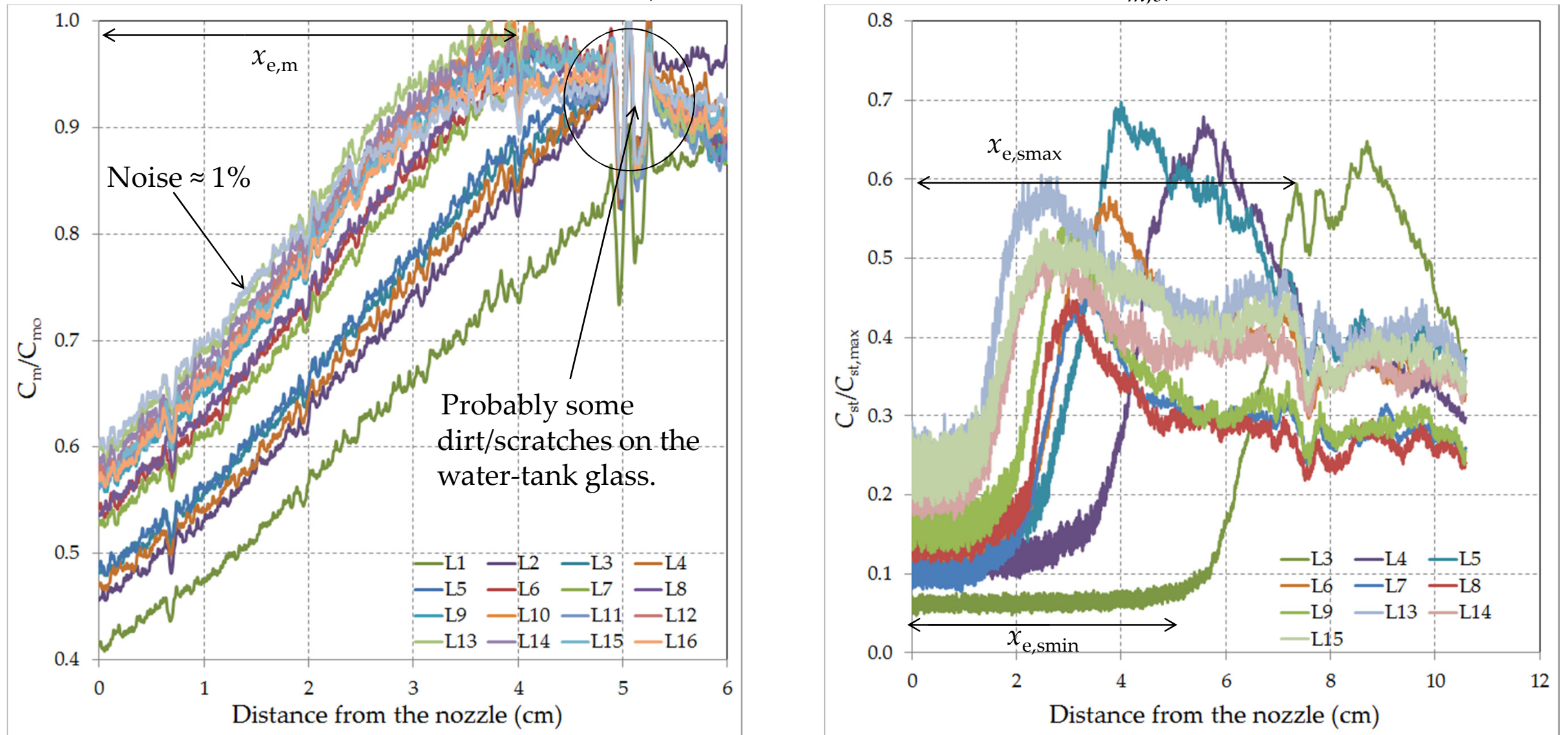


Figure 6: Mean  $C_m$  (left) and standard deviation  $C_{st}$  (right) distributions (normalized with their maximum values  $C_{m0}$  and  $C_{st,max}$ , respectively) along the jet-axis, from the 1<sup>st</sup> experiment ( $D=0.5$  cm). For Li see section 7.

## 8c. Experimental results (graphs)

Graphs with all the measured ZFE lengths are presented below. It is observed that as  $Re$  increases, distance  $x_e$  decreases (with the exception of  $x_{e,m}$  and  $x_{e,smax}$  of the 3<sup>rd</sup> experiment). Also, the distances  $x_{e,smin}$  and  $x_{e,smax}$  seem to be anti-symmetrical with respect to  $x_{e,m}$ .

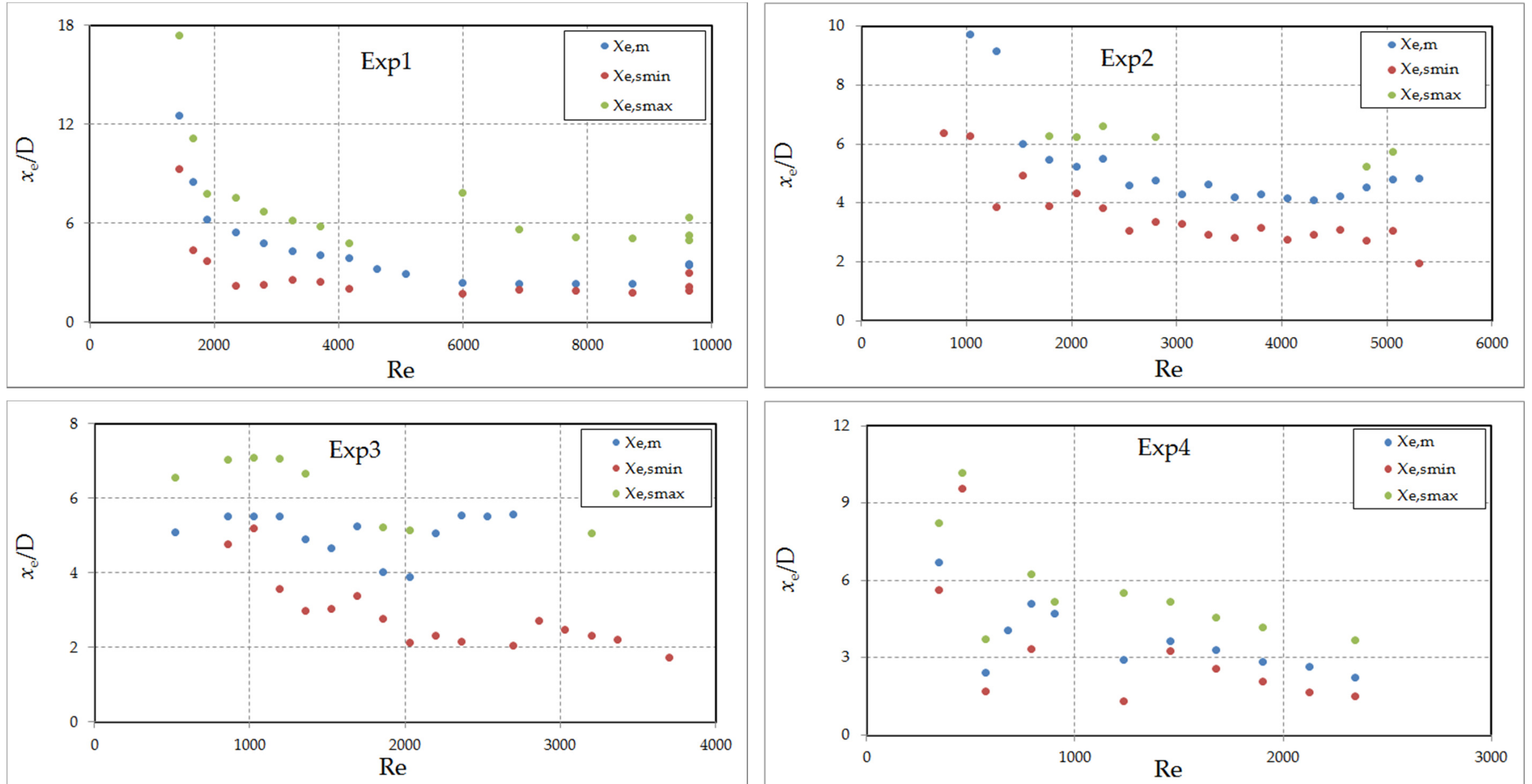


Figure 7: Measurements of the ZFE length versus Reynolds number taken from the experiments described above. Only values of green and yellow (symbolized with ^) labels are presented.

# 9. Conclusions

The main conclusions of this work are as follows:

- The RMS image is much clearer than the time-averaged one, concerning the ZFE outer limit.
- The ZFE, defined through maximum RMS, seems to have a ballistic geometrical shape. Also, transition to turbulence seem to occur at the jet nozzle elevation.
- It is generally observed that as the Reynolds number increases, the ZFE length decreases.
- The present measurements of the ZFE are quite different than those proposed in earlier studies.

## Acknowledgements

We acknowledge the free, collaborative and multilingual Internet encyclopedia Wikipedia (supported by the non-profit Wikimedia Foundation) for offering us some first scientific glances in several topics (from ISO notations to LIF techniques) and thus, saving us valuable time.

## References

- Abramovich G.N., 'The Theory of Turbulent Jets', *MIT Press*, ch. 5.1, p. 352-357, 1963,.
- Albertson M. L., Y. B. Dai, R. A. Jensen and H. Rouse, Diffusion of Submerged Jets, 74. p. 639 – 664., 1948.
- Chen J. & C.P. Nikitopoulos, 'On The Near Field Characteristics Of Axisymmetric Turbulent Buoyant Jets In A Uniform Environment', *Int. J. Heat Mass Transfer.*, Vol. 22, p. 245-255, 1979.
- Crow, S.C. and Champagne, F.H., Orderly structure in jet turbulence, *J. Fluid Mech* Vol. 48, pp.547–596., 1971.
- Ferrier A.J., Funk D.R., and Roberts P.J.W.. 'Application of optical techniques to the study of plumes in stratified fluids', *Dynamics of Atmospheres and Oceans*, Vol. 20, p. 155-183, 1993.
- Jirka G.H., 'Integral Model for Turbulent Buoyant Jets in Unbounded Stratified Flows. Part I: Single Round Jet', *Environmental Fluid Mechanics*, Vol. 4, p. 1–56, 2004.
- Henderson-Sellers B., 'The zone of flow establishment for plumes with significant buoyancy', *Appl. Math. Modelling*, Vol. 7, 1983
- Hongwei W, Investigations of buoyant jet discharges using combined DPIV and PLIF. PhD thesis in Civil and Structural Engineering, Nanyang Technological University, Singapore, 2000
- Kwon S. J. & I.W. Seo, 'Reynolds number effects on the behavior of a non-buoyant round jet', *Experiments in Fluids*, Vol. 38, p. 801–812, 2005.
- Labus T.L. & E.P. Symons, 'Investigation Of An Axisymmetric Free Jet With An Initially Uniform Velocity Profile', *Lewis Research Center*, NASA Technical Note D-6783, 1972.
- Lee H.W. & G.H. Jirka, 'Vertical round buoyant jet in shallow water', *Journal of the Hydraulics Division*, Proc. ASCE, 107(HY12), p. 1651-1675, 1981.
- Pratte B.D. & W.D. Baines, 'Profiles of the Round Turbulent Jet in a Cross Flow', *ASCE Journal of the Hydraulics Division*, 92, HY6, 5556, 1, p. 53-64, 1967.
- Schatzmann M., 'The Integral Equations of Round Buoyant Jets in Stratified Flows', *J. Appl. Math. Phys. (ZAMP)*, Vol. 29, N. 4, p. 608-630, 1978.
- Walker D.A., 'A Fluorescence Technique for Measurement of Concentration in Mixing Liquids', *J. Phys E: Sci Instrum*, Vol. 20, p.217–224A, 1987.
- Xu G. Antonia RA. 'Effect of different initial conditions on a turbulent round free jet' *Exp Fluids*, Vol. 33, p. 677–683, 2002.